Characterization of the flow past real road vehicles with blunt afterbodies

M Grandemange, D Ricot, C Vartanian, T Ruiz, Olivier Cadot

Characterization of the flow past real road vehicles with blunt afterbodies

M. Grandemange,[1,2] D. Ricot,[3] C. Vartanian,[4] T. Ruiz,[2] and O. Cadot[1]

[1] *Unité de Mécanique, Ecole Nationale Supérieure de Techniques Avancées, ParisTech, Chemin de la Hunière, 91761 Palaiseau Cedex, France*
[2] *PSA Peugeot Citroën, Centre Technique de Velizy, Route de Gisy, 78943 Vélizy-Villacoublay Cedex, France*
[3] *Renault, Technocentre, 1 avenue du Golf, 78288 Guyancourt Cedex, France*
[4] *GIE S2A, Souffleries Aéroacoustiques Automobiles, 2 avenue Volta, 78180 Montigny Le Bretonneux, France*

The flow past two different road vehicles with blunt afterbodies is studied at a Reynolds number based on the vehicle length of 10^7. The boundary layer thickness and the pressure distribution around the body are characterized. Then, the wake is investigated through static pressure and velocity measurements. Similar properties are obtained for both vehicles, in particular the lowest pressure on the after-body is reported on the lower part of the base. Hot-wire anemometry is also used to depict the dynamics of the flow. The detached shear from the roof behaves as free shear turbulent flows whereas the flow from the underbody rather corresponds to homogeneous shear turbulent flows. In addition, global mode dynamics is reported in the wake of one vehicle and is associated with an antisymmetric coupling of the lateral mixing layers. However, the intensity of this mode is limited and it may not be a contributor to the drag since its maximum of amplitude is downstream the recirculation bubble. Eventually, these results are analyzed to orient future drag reduction control strategies.

I. INTRODUCTION

The drag force resulting from flow over road vehicles is responsible for a dominant part of the fuel consumption, especially over 30 m s^{-1}. During the last decades, the growing energetic constraints have then motivated research activities to improve the understanding of fundamental notions such as stability or force intensities in the wake of simplified vehicles. The objective is often to limit the drag through optimization of the geometry or flow control. The work of Ahmed *et al.*[1] paved the way to the comprehension of the structures of the flow around different shapes of road vehicles. Indeed, they proved the critical influence of the rear shape on a simplified vehicle. For moderate slant angles (from 12.5° to 30°), a pair of intense counter-rotating vortices develops in the wake of the model reducing the base pressure[2]. In the worst case (slant angle close to 30°), these structures induce up to 45% increase in drag in comparison to the 0° case. Since similar flow structures are reported in the wakes of notch-back and fast-back vehicles[3], important work is devoted to the drag reduction of the 25° slant angle body. Thus, various passive and active control strategies are reported in literature such as splitter plates[4], flaps[5,6], boundary layer steaks[7] or even pulsed jet[8]. On the other hand, for slant angles below 10°, the topology is characterized by a massive recirculation bubble in the wake. This recirculating flow, associated with low levels of base pressure, is the major contributor to the aerodynamic drag. Then, the use of different control devices as splitter plates[9], chamfer[10] or porous devices[11] may limit the base drag of this square-back case. However, once transposed on real vehicles, such devices often have a reduced efficiency partially because the natural flow remains particularly unclear. For example, if characteristic wake frequencies are reported[12,13] over simplified geometries, the presence of global modes in the wake of real vehicles is still an open issue.

Therefore, the present work aims at clarifying the flow past two different blunt vehicles: a commercial van and a compact crossover. To our knowledge, the description of the separations and global mode dynamics in the wake of real cars has not been reported in the literature. Thus, the results are to be used as a lacking reference and the present analyses should be considered to develop the efficient flow control strategies needed by industry or to validate new development in terms of numerical simulations.

The article is organized as follows. In Section II, the experimental setup and measurements are presented. Then, Section III is devoted to the results: analysis of the boundary layers (III A), base pressure measurements (III B), characterization of the mean flow in the wake (III C), focus on the mixing layer activity (III D) and investigation of global mode dynamics (III E). The contributors to the aerodynamic drag are discussed in section IV. Eventually, concluding remarks are presented in section V.

II. EXPERIMENTAL SET-UP

A. Wind tunnel and vehicles

The experiments are performed in the full scale aeroacoustic wind-tunnel of GIE S2A at Montigny-Le-Bretonneux[14]. The test section is a 3/4 open jet with a cross section of 24 m^2. Four wheel spinners and a central rotating belt enable to operate under rolling road conditions. The inlet and the moving belt velocities are set at 33.3 m s^{-1}. The Reynolds number based on the length L of the vehicles is close to 10^7.
The flow is investigated past two different passenger vehicles with a blunt after-body: a Renault Trafic and a Peugeot 3008 (see Fig. 1). The dimensions of the vehicles are presented in Table I. The first geometry is a commercial vehicle so its cubic geometry is due to its function. The originality of its shape is the small hump at the junction of the windshield and the roof, just above the heads of the front passengers. The second vehicle has also a blunt after-body but its shape is slightly different in particular regarding the inclination of the roof.
The coordinate system is defined as $\vec{e_x}$ oriented along the free flow direction, $\vec{e_y}$ in the vertical direction and $\vec{e_z}$ forming a direct coordinate system. The origin is set on the floor in the middle of the vehicles in the z direction and at the maximum x coordinate of the vehicle. Δi is the algebraic distance in the i direction to a given reference point such as the separation from the roof or a surface. The velocities are defined as $\vec{u} = u.\vec{e_x} + v.\vec{e_y} + w.\vec{e_z}$; $u_{ij} = \sqrt{u_i^2 + u_j^2}$ is the amplitude of velocity at the considered point in the plane ($\vec{e_i}$,$\vec{e_j}$). $A = Mean(a)$ and $Std(a)$ are respectively average value and standard deviation of any quantity a. The density ρ and inlet velocity U_0 are used to obtain non-dimensional values marked with an asterisk.
The GIE S2A complex provides measurements systems to study the flow around the vehicles; they are presented in Section II B.

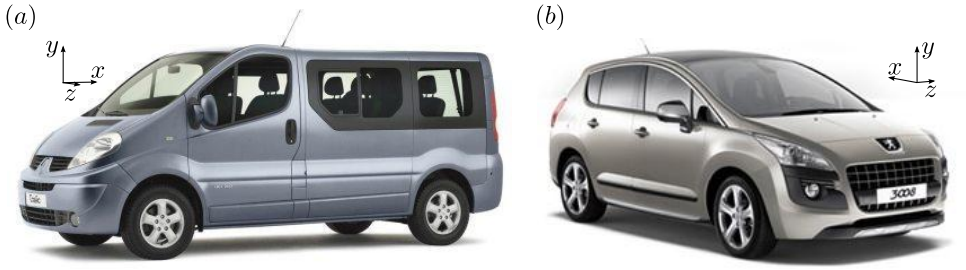

Figure 1: Blunt vehicles studied in the wind tunnel: Renault Trafic (a) and Peugeot 3008 (b).

	L (mm)	W (mm)	H (mm)
Renault Trafic	4782	1904	1942
Peugeot 3008	4365	1837	1639

Table I: Total length, width (side mirrors excluded) and height (resp. L, W and H) of the different models.

B. Measurement systems

The pressure on the vehicles are obtained using parietal pressure taps. In the flow, a 18 hole probe mounted on a three-axis robot enable the measurement of the mean velocities U_x, U_y and U_z as well as the static and total pressures. The pressure is considered through C_p defined as

$$C_p = \frac{p - p_0}{\frac{1}{2}\rho {U_0}^2}. \quad (1)$$

The automatic displacement and recording is implemented to get these data in different planes iso-x, iso-y or iso-z. The displacement system can also support a 1D hot-wire probe system. The velocity in the plane ($\vec{e_x}$,$\vec{e_y}$) is then

measured with a time resolution better than 1 kHz enabling power spectrum analyses at least up to 500 Hz wherever wanted around the vehicles. Velocity signals are recorded during several minutes and power spectra are time averaged over windows of 1 s or 10 s depending on the signal duration. This averaging over windows is denoted by "$\langle ... \rangle$". Auto and cross correlations between two hot-wire probes at different locations are equally performed. $\xi_F(f)$ stands for the Fourier transform of the function ξ evaluated at the frequency f and $\overline{\xi}(f)$ for its complex conjugate. The coherence r and phase ϕ between the simultaneous signals $a(t)$ and $b(t)$ are defined as modulus and argument of γ defined in (2).

$$\gamma(f) = \frac{\langle a_F(f) \cdot \overline{b_F}(f) \rangle}{\sqrt{\langle |a_F(f)|^2 \rangle \langle |b_F(f)|^2 \rangle}} = r(f) e^{i\phi(f)}. \tag{2}$$

III. RESULTS

A. Boundary layers

The boundary layer has been characterized using the 1D hot-wire probe mounted on the displacement system. Four profiles on the roof in the plane $z = 0$ m are presented in Figure 2 at 0.15, 0.5, 1.0 and 1.5 m upstream the roof end for the Renault Trafic. The corresponding results on the Peugeot 3008 are plot in Figure 3. The characteristic thicknesses are presented in Table II. To avoid the aerodynamic disturbances from the antenna on the Peugeot 3008, the measurements are systematically performed in the plane $z = 0.12$ m rather than at $z = 0$ m.

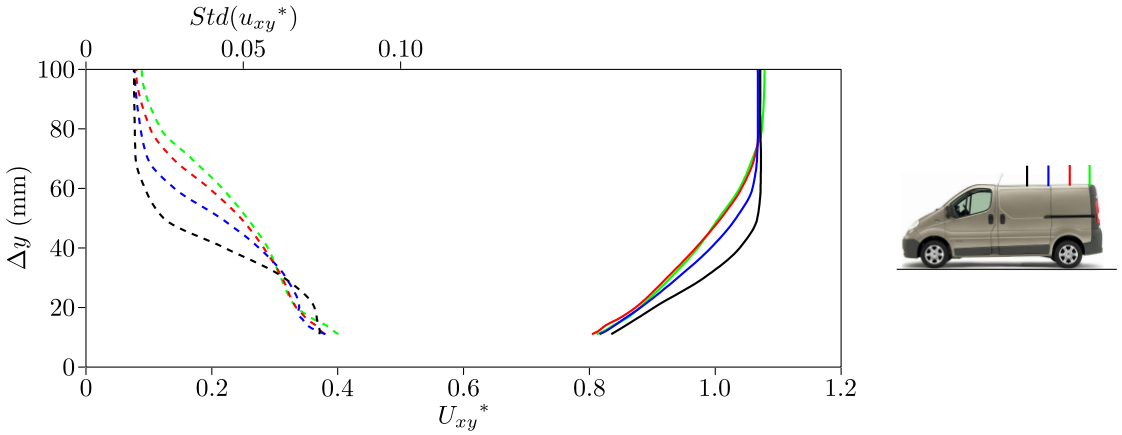

Figure 2: Mean (continuous lines) and fluctuating (dashed lines) velocity profiles of the boundary layer on the roof of the Renault Trafic in the plane $z = 0$ m: $\Delta x = -1.5$ m, black lines; $\Delta x = -1.0$ m, blue lines; $\Delta x = -0.5$ m, red lines; $\Delta x = -0.15$ m, green lines. Δx and Δy are respectively the algebraic distances to the roof end and to the roof surface.

	Renault Trafic			Peugeot 3008		
Δx (mm)	δ_{99} (mm)	δ_* (mm)	θ (mm)	δ_{99} (mm)	δ_* (mm)	θ (mm)
-1500	46±0.5	9.5±0.2	5.3±0.2	–	–	–
-1000	58±0.5	11.0±0.2	6.4±0.2	32±0.5	7.3±0.2	3.4±0.2
-500	69±0.5	12.2±0.2	7.4±0.2	47±0.5	8.7±0.2	4.6±0.2
-150	74±0.5	12.6±0.2	7.7±0.2	–	–	–
-50	–	–	–	73±0.5	13.6±0.2	7.8±0.2

Table II: Boundary layer characteristics on the roof of the Renault Trafic and on the Peugeot 3008 respectively in the plane $z = 0$ m and $z = 0.12$ m: δ_{99}, thickness based on 99% of free-stream velocity; δ_*, displacement thickness; θ, momentum thickness.

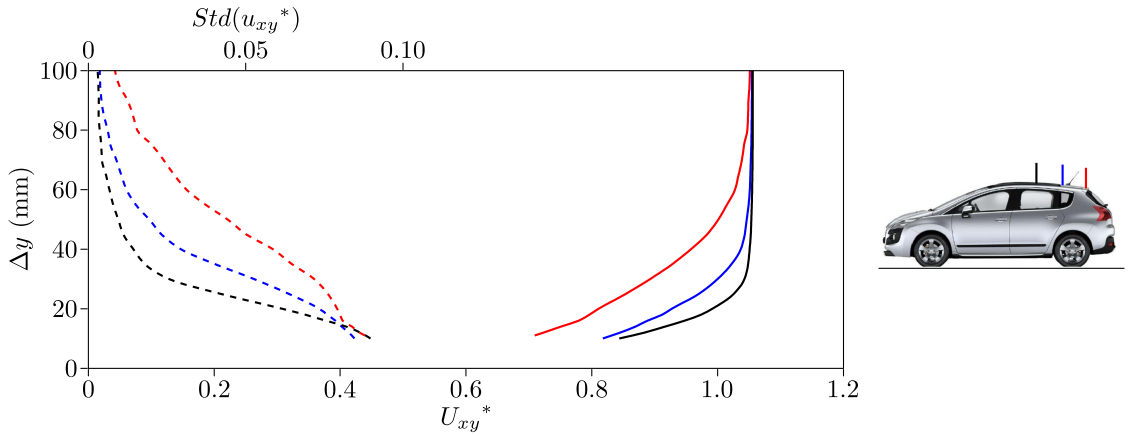

Figure 3: Mean (continuous lines) and fluctuating (dashed lines) velocity profiles of the boundary layer on the roof of the Peugeot 3008 in the plane $z = 0.12$ m: $\Delta x = -1.0$ m, black lines; $\Delta x = -0.5$ m, blue lines; $\Delta x = -0.05$ m, red lines. Δx and Δy are respectively the algebraic distances to the roof end and to the roof surface.

The boundary layers just before the roof separation have very similar characteristic thicknesses: $\delta_{99} \approx 70$ mm. However, the associated evolutions are distinct: the boundary layer has a linear growth on the Renault Trafic while it grows much faster on roof of the Peugeot 3008. This is certainly due to the difference in the roof inclinations: the Renault Trafic has an horizontal roof whereas the Peugeot 3008 present a smooth shape inducing adverse pressure gradients along the roof. There may also be a role of the roughness of the surface on the Renault Trafic.

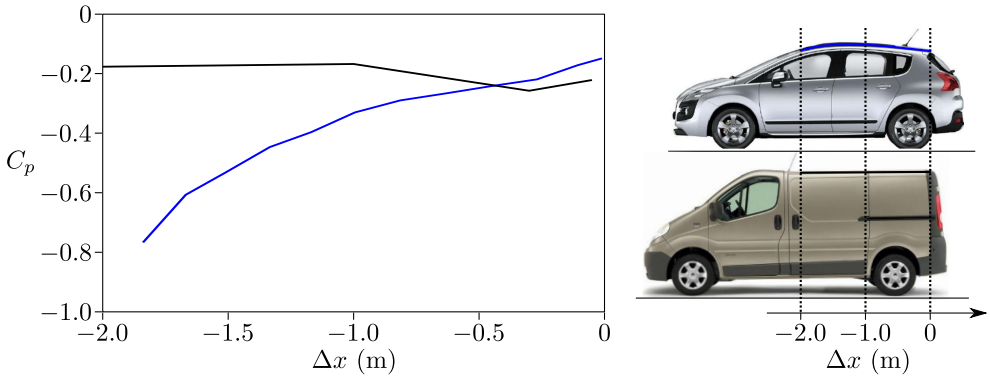

Figure 4: Distribution of static pressure on the roof of the Renault Trafic (black line) and of the Peugeot 3008 (blue line). Δx is the algebraic distances to the roof end.

The static pressure distributions on the roof in the plane $z = 0$ m are shown in Figure 4 for both vehicles. On the Renault Trafic, the static pressure is constant in the range -2 m $< \Delta x < -1$ m. There is then a decrease followed by an increase of pressure just before the massive separation at the roof end, this evolution must be related to the chamfered shape of the roof end. A similar evolution is observed on the sides of this commercial vehicle (measurements not shown in this paper). On the contrary, there is a regular increase of pressure from the end of the windshield to the roof end on the Peugeot 3008. The inclination of the roof leads to a decrease of velocity resulting in pressure recovery.
The static pressure at the roof end is a critical parameter as it is correlated with the level of pressure on the base. These levels of base pressure are presented in the Section III B.

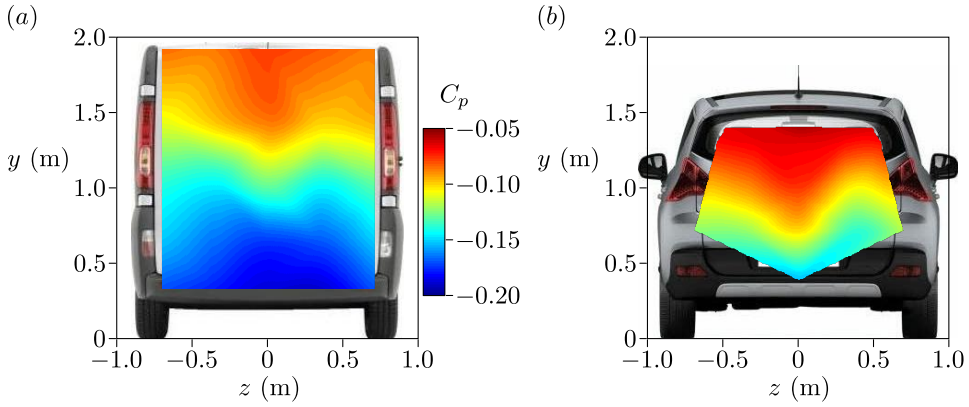

Figure 5: Distribution of static pressure on the base of the Renault Trafic (a) and of the Peugeot 3008 (b).

B. Base pressure

Parietal pressure sensors have been placed on the rear part of the vehicles to get the pressure signature displayed in Figure 5. The pressure levels on the two vehicles have a similar repartition. The average levels are slightly larger on the base of the Peugeot 3008 than on the Renault Trafic as expected from the C_p measurements presented in Figure 4. The measurement is almost independent of z whereas there are important gradients in the y direction. The pressure in the upper region of the base is close to -0.05, there is a continuous decrease of pressure up to almost -0.20 at the lower part of the base.
This low value may result from the under-body roughness and from the ground presence. To argue on this point, distributions of pressure and velocities in the recirculating flow are considered in Section III C.

C. Recirculation region

The topologies of the wakes are obtained in the planes $z = 0$ m and $x = 1.0$ m in the wake of the Renault Trafic and $z = 0.12$ m and $x = 0.5$ m in the wake of the Peugeot 3008, the measurement system gives access to the mean velocity in the three directions and to the static pressure.
The distributions of pressure in planes $(\vec{e_x},\vec{e_y})$ are shown in Figure 6. The low pressure region close to the base is clearly visible. Further downstream, the pressure increases to reach positive values after the recirculation closure. As expected from the pressure measurements on the base of the vehicles, the pressure distributions in the recirculation region strongly depend on the y position.
The associated flow velocities in planes $(\vec{e_x},\vec{e_y})$ are presented in Figure 7. On both vehicles, the pressure gradients in the y direction is associated with a diagonal recirculating flow. The whole recirculation bubble is fed by the flow coming from the under-body which is confirmed by the streamlines in cross-flow planes (see Figure 8). Actually, inside the recirculating flow marked by the iso-contour ${U_x}^* = 0$ delimiting the back flow, the streamlines are vertical, *i.e.* $U_y \gg U_z$. In addition, the contours of U_x preserves roughly the shape of the base. The main difference is the reduced height of the wake of the Peugeot 3008 as the inclination of the roof makes the flow to separate with an approximate angle of 8° referring to the x direction (compare Figures 8a and b). On the contrary, the separations occur aligned to the stream-wise direction on the side and bottom faces of the Peugeot 3008 and on the four faces of the Renault Trafic.
Only half cross-flow planes are presented but the result is not expected to be perfectly symmetric since the vehicles do not strictly respect the reflectional symmetry: air cooling of the engine, under-body roughness... In addition, even if not observed during these experiments, cases of reflectional symmetry breaking in three dimensional wakes may appear even at high Reynolds[15]. Reflectional symmetry breaking has also been observed by the CNRT R2A for the square back Ahmed body at $\mathrm{Re} = 10^7$ in the full scale aeroacoustic wind-tunnel of GIE S2A.
Eventually, a particularity in the streamlines downstream the Renault Trafic is observed in Figure 7. Three stagnation points at $x = 1.8$ m are reported: two saddle points ($y = 0.65$ m and 1.55 m) and one source point ($y = 1.1$ m), whereas the Peugeot 3008 has classically one saddle point at $x = 1.1$ and $y = 1$ m. This wake organization might be an indicator of bistable flow as presented in the experiments of Grandemange *et al.*[16]. However such phenomenon has not been identified and may rather rely on the intrusion of the probe mounted on the displacement system.

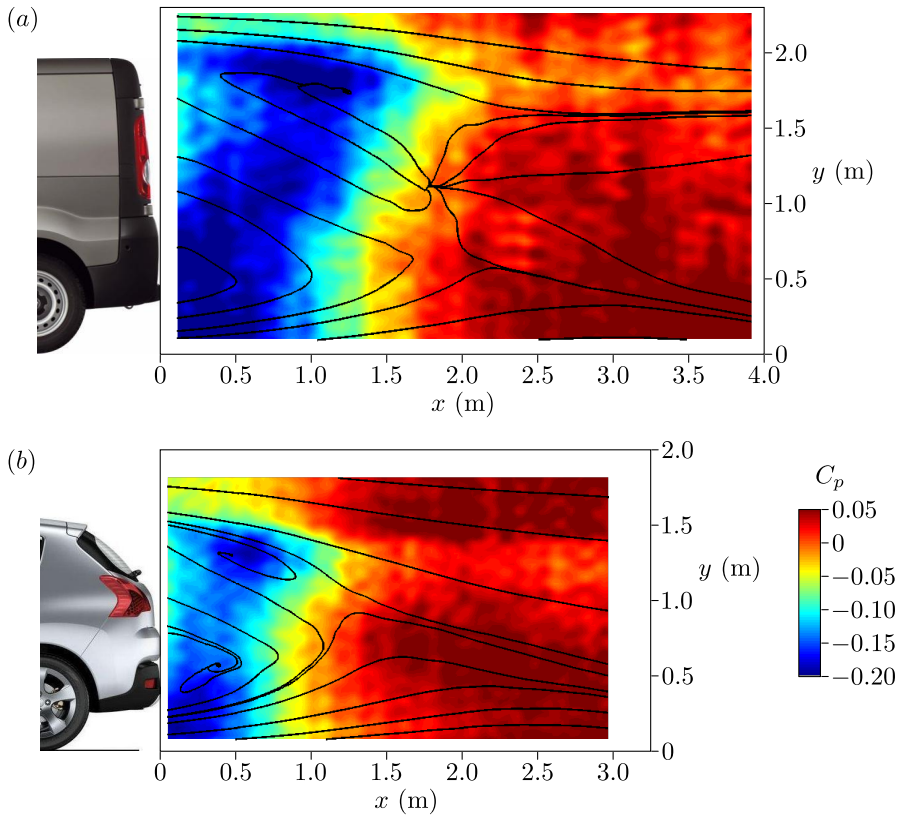

Figure 6: Distribution of static pressure and streamlines in the wake of the Renault Trafic in the plane $z = 0$ m (a) and of the Peugeot 3008 in the plane $z = 0.12$ m (b).

D. Mixing layer

To characterize the differences in the flow coming from the roof and the under-body, hot-wire measurements are performed in the top and bottom mixing layers. Velocity profiles at different downstream positions x are measured and the position of the mixing layer is marked in the y direction by the contours y_α defined as

$$U_{xy}(x, y_\alpha) = \alpha U_0. \tag{3}$$

The size of the mixing layer δ_m is then deduced as

$$\delta_m = |y_{0.9} - y_{0.1}|. \tag{4}$$

The position of the maximum of the velocity fluctuations at a given x is denoted by y_{rms}.
The mixing layer downstream the roof is first considered. In Figure 9, its growth is almost linear at least up to 1 m after the separation. The growth rate $\mathrm{d}\delta_m/\mathrm{d}x$ is respectively measured at 0.14 and 0.12 for the upper mixing layer of the Renault Trafic and of the Peugeot 3008. This linear growth is a characteristic of free shear turbulent flows[17,18] where the growth rate depends on the state of the flow at the separation and ranges between 0.06 and 0.11. The larger value obtained here might be ascribed to the thick turbulent boundary layer that develops on the roof. The second common characteristic with turbulent free shear flows is that the mixing layer spreads preferentially into the low velocity region[19]. In Figure 9 the contour of $y_{0.9}$ is parallel to the external flow, *i.e.* along the x direction on the Renault Trafic and slightly oriented due to the inclination of the roof on the Peugeot 3008. Past roughly 0.2 m downstream the separation of the roof, the contour $y_{0.5}$ is located right between $y_{0.1}$ and $y_{0.9}$ so that the vorticity initially concentrated near the wall of the roof spreads rapidly to reach a symmetric distribution over the mixing

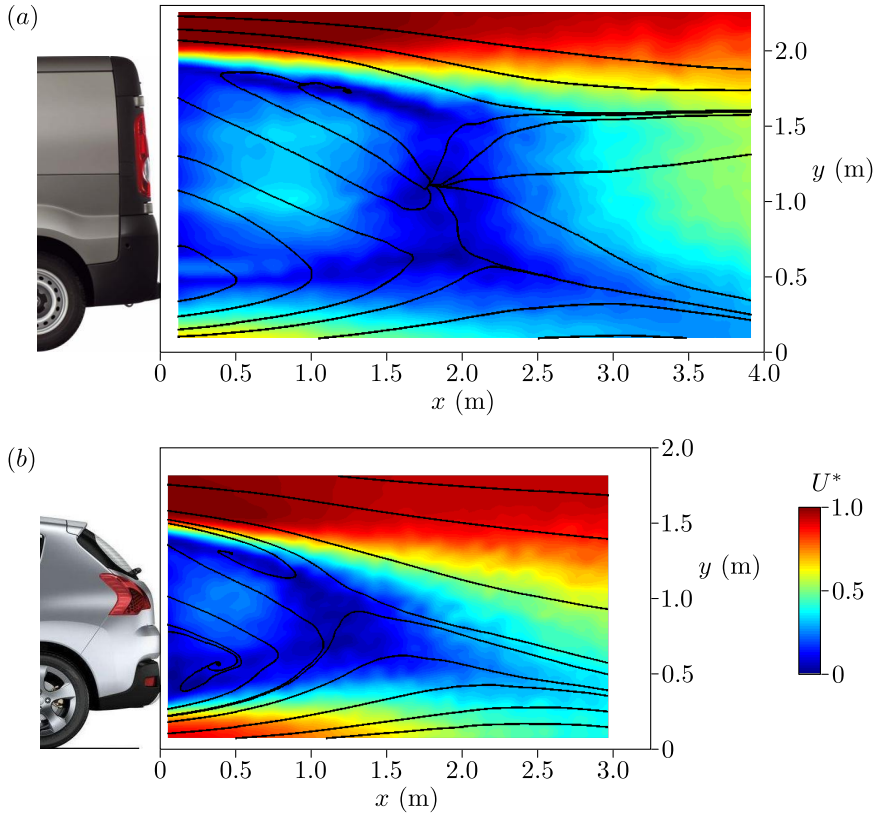

Figure 7: Distribution of velocity and streamlines in the wake of the Renault Trafic in the plane $z = 0$ m (a) and of the Peugeot 3008 in the plane $z = 0.12$ m (b).

layer. It is observed that the contours of y_{rms} and $y_{0.5}$ are superimposed so that the activity of the mixing layer is maximal in the middle the shear layer. This point is clarified by the distribution of the velocity fluctuations in the mixing layers presented in Figure 10.
Similar measurements have been performed in the mixing layer from the Peugeot 3008 under-body. The size of the mixing layer is close to the ground clearance partially due to the under-body roughness of the vehicle and the evacuation of flow devoted to the engine cooling. The growth is not linear but the expansion remains oriented toward the recirculating region. The mixing layer activity is equally centered on $y_{0.5}$ and the intensity of the velocity fluctuations is slightly lower than the one measured in the upper mixing layer. In the wake of the Renault Trafic, the velocities presented in Figure 7(a) point out that the velocity is reduced right downstream the under-body and that vorticity is equally distributed over the ground clearance height.

The auto-power spectra of the velocity signals in the upper mixing layers at y_{rms} for different x positions are presented in Figure 11. They all show an almost constant distribution of energy corresponding to the large scale structures of turbulence below a characteristic frequency f_c (10 Hz to 20 Hz depending on x) and the distribution of energy decreases with a $-5/3$ power law as expected by the Kolmogorov theory for the inertial range of turbulence.
Studying the evolution in the stream-wise direction, the result presented in Figure 11 shows that the characteristic frequency of the spectra f_c separating the large scales and the inertial ranges, decreases as x increases. This indicates that this frequency is based on the local thickness of the mixing layer : $f_c \sim U_0/\delta_m$ which is also a characteristics for turbulent free shear flows[20].
The auto-power spectra from the bottom mixing layer visible in Figure 12 present the exact same repartition of energy but the characteristic frequency $f_c \approx 10$ Hz is independent of x. Then the size and activity of the mixing layer right downstream the under-body is similar to the one from the roof but 1 m downstream the separation. In parallel, these two regions where the mixing layers become unstructured correspond to the locations where the pressure is minimal on the wake (see Fig. 6).

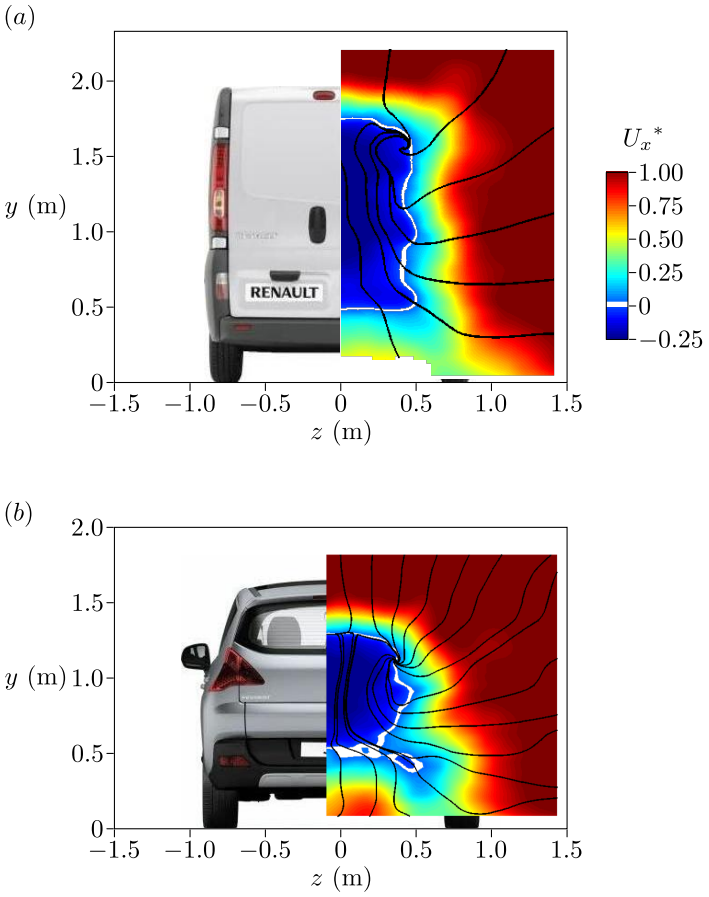

Figure 8: Distribution of velocity and streamlines in the wake of the Renault Trafic in the plane $x = 1$ m (a) and of the Peugeot 3008 in the plane $x = 0.5$ m (b).

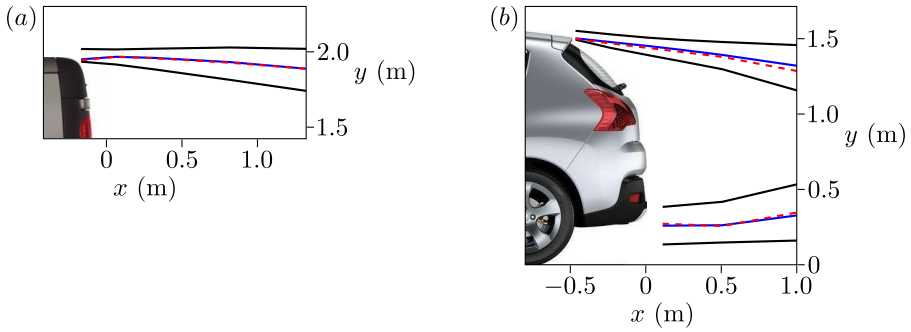

Figure 9: Positions of the contours $y_{0.1}$ and $y_{0.9}$ (back lines), $y_{0.5}$ (blue lines) and y_{rms} (red lines) in the mixing layers of the Renault Trafic (a) and the Peugeot 3008 (b) from hot-wire measurements.

E. Global mode dynamics

The presence of a synchronized dynamics, *i.e.* global modes, is now studied in the wake of these two vehicles using two hot-wire signals.

In the flow over the Peugeot 3008, no peak of energy is reported in the spectral repartition of energy. Wherever the probe is located, the results are similar to the one presented in Figure 13. As for spectra in the mixing layer detailed in Section III D, there is a characteristic frequency $f_c \approx 10\ Hz$ from which the inertial range of turbulence starts. Note that f_c is always measured around 10 Hz except in the close wake mixing layer as presented in Figure 11(b).

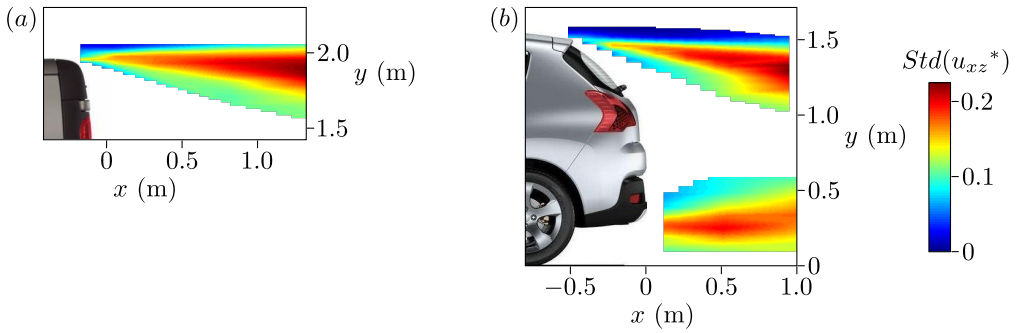

Figure 10: Distribution of the velocity fluctuations in the mixing layers of the Renault Trafic (a) and the Peugeot 3008 (b) from hot-wire measurements.

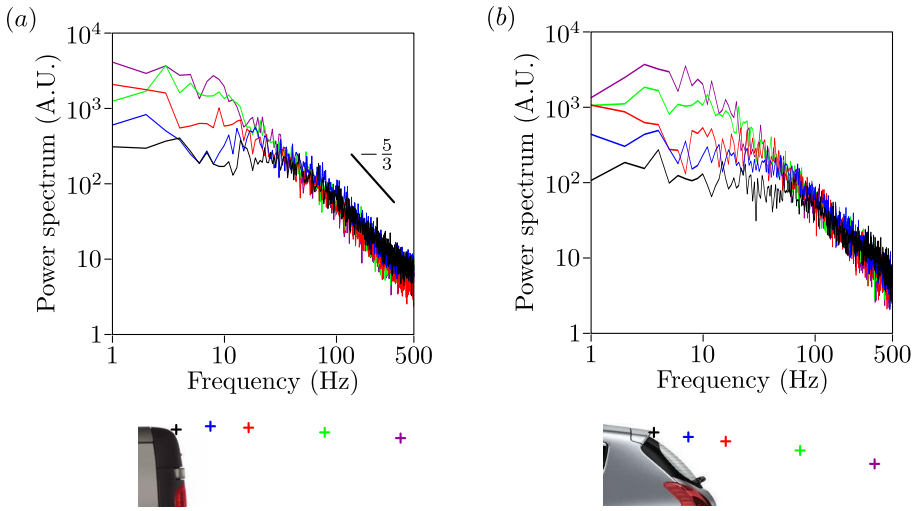

Figure 11: Auto-power spectra in the mixing layer from the roof of the Renault Trafic (a) and of the Peugeot 3008 (b) at the maximum of fluctuating velocities at $\Delta x = 0.02$ m (black line), $\Delta x = 0.25$ m (blue line), $\Delta x = 0.5$ m (red line), $\Delta x = 1.0$ m (green line) and $\Delta x = 1.5$ m (purple line). Δx is the algebraic distances to the roof end.

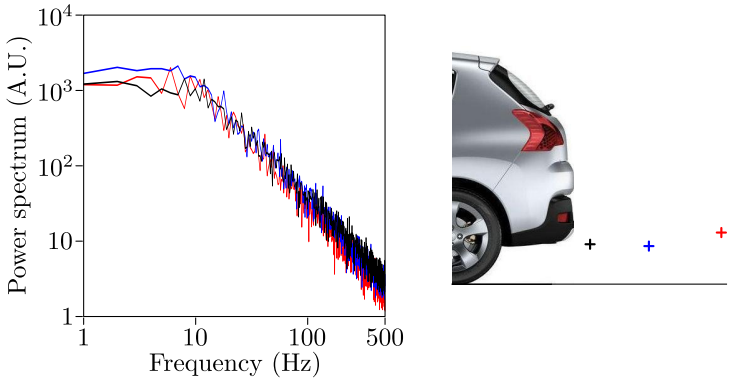

Figure 12: Auto-power spectra in the mixing layer from the under-body of the Peugeot 3008 at the maximum of fluctuating velocities at $x = 0.1$ m (black line), $x = 0.5$ m (blue line) and $x = 1.0$ m (red line).

This value of 10 Hz appears to be the frequency associated with the large scale structures of turbulence of the whole wake.

On the contrary, in the flow past the Renault Trafic, some coherent motion of the wake are reported. Indeed, the

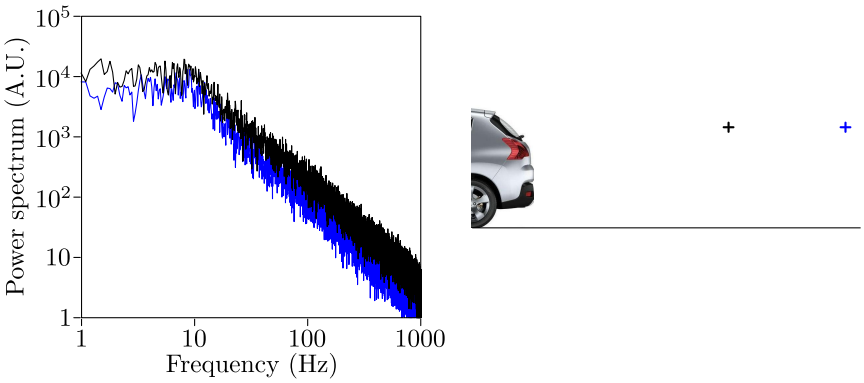

Figure 13: Autopower spectra in the wake of the Peugeot 3008 at (2.5 m, 1.3 m, 0 m) (black line) and (4.0 m, 1.3 m, 0 m) (blue line).

auto-power spectra of the velocity signals at (4.0 m,1.0 m,±0.3 m) plot in Figure 14(a) present peaks of energy at $f_{GM} = 4$ Hz. To precise the structure of this mode, cross-correlations between these two simultaneous signals are performed. It shows that the coherence reaches 0.7 at 4 Hz and corresponds to an antisymmetric mode in the z direction since the signals are in phase opposition. Only 0.6 m separate the probes which is small compared that of the vehicle width but corresponds to the wake width at this location. Once normalized by W, f_{GM} corresponds to a Strouhal number $\mathrm{St_{GM}} = fW/U_0 = 0.23$.

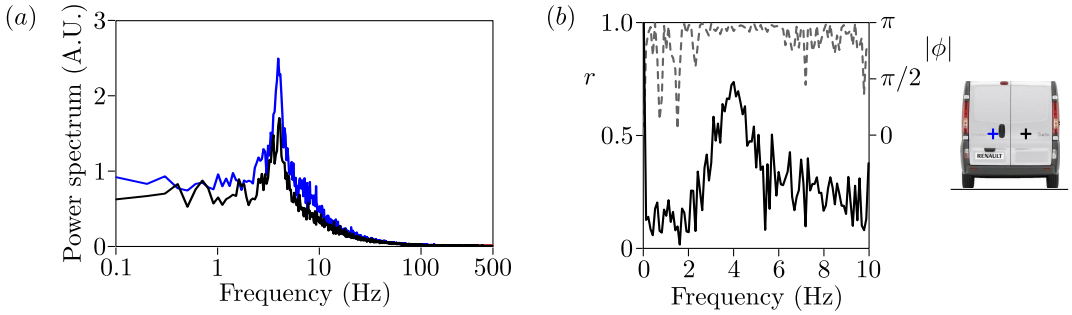

Figure 14: (a) Auto-power spectra in the lateral mixing layers from the Renault Trafic at (4.0 m,1.0 m,0.3 m) (black line), (4.0 m,1.0 m,-0.3 m) (blue line). (b) Correlation (left scale, continuous line) and phase (right scale, dashed line) between the velocity signals at (4.0 m,1.0 m,0.3 m) and (4.0 m,1.0 m,-0.3 m).

Auto-power spectra even much closer to the base at (0.4 m,1.8 m,0.7 m) and (0.4 m,1.8 m,-0.7 m) reports the same coherent structure at $f_{GM} = 4$ Hz with a coherence close to 0.5 and a phase opposition (see Fig. 15). Thus this peak of energy corresponds to a global mode. However, it is not reported everywhere in the wake. For example, the auto-power spectra and the cross-correlation analyzes performed at $x = 2$ m that could easily measure a lateral or a vertical oscillation of the wake at the end of the recirculation, do not report any significant coherent motion (see Figs. 16 and 17). In Figure 16(a), a slight increase of energy is measured around f_{GM} at (2.0 m,1.8 m,0 m) but is not as clear as in Figures 14 and 15. As a result, this mode seems to develop from the interaction of the lateral mixing layers mostly from the upper part of the vehicle. Then it persists downstream and is particularly visible at $x = 4$ m which corresponds to two times the characteristic width or height of the vehicle.
The exploration of the envelop of this mode in the wake is very difficult to achieve since the resolution of the activity at 4 Hz requires spectral analyses over windows of 10 s. In addition, to get converged distribution of energy, the averaging denoted "$\langle ... \rangle$" need to be performed over a sufficient number of windows so that each velocity signal is recorded over at least 500 s which is an important cost regarding the use of this industrial wind-tunnel.

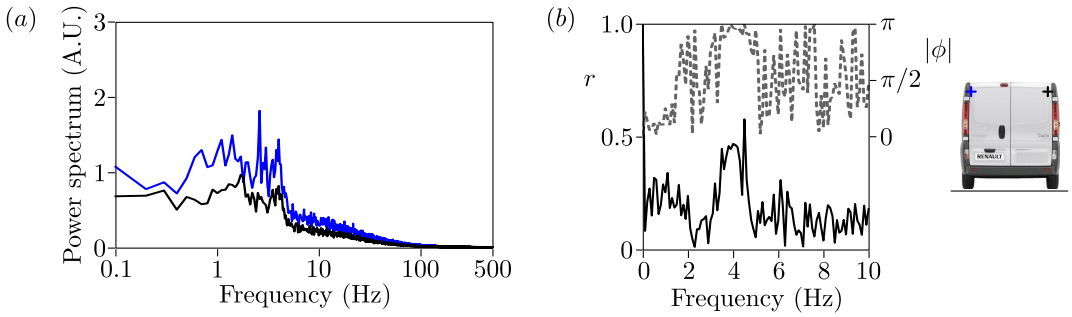

Figure 15: (*a*) Auto-power spectra in the lateral mixing layers from the Renault Trafic at (0.4 m,1.8 m,0.7 m) (black line), (0.4 m,1.8 m,-0.7 m) (blue line). (*b*) Correlation (left scale, continuous line) and phase (right scale, dashed line) between the velocity signals at (0.4 m,1.8 m,0.7 m) and (0.4 m,1.8 m,-0.7 m).

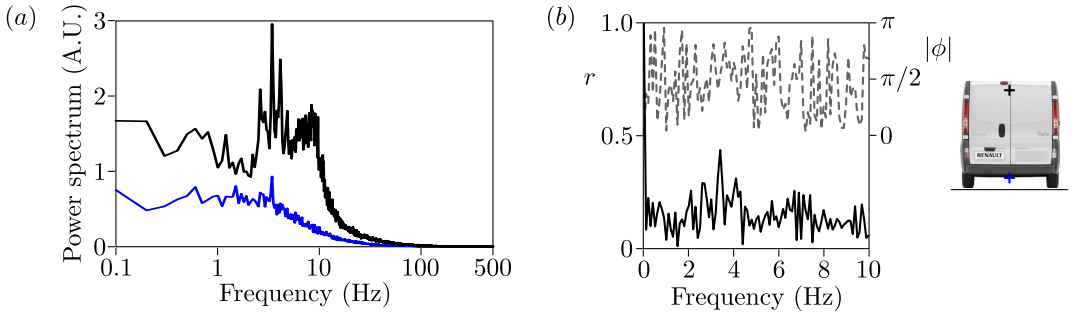

Figure 16: (*a*) Auto-power spectra in the top and bottom mixing layers from the Renault Trafic at (2.0 m,1.8 m,0 m) (black line), (2.0 m,0.2 m,0 m) (blue line). (*b*) Correlation (left scale, continuous line) and phase (right scale, dashed line) between the velocity signals at (2.0 m,1.8 m,0 m) and (2.0 m,0.2 m,0 m).

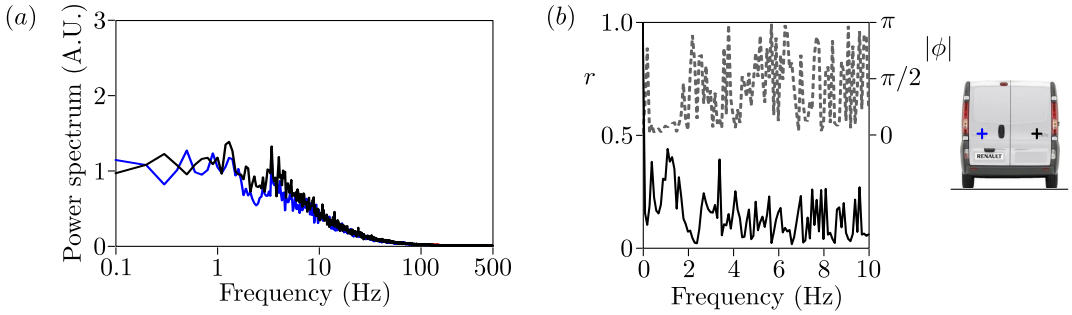

Figure 17: (*a*) Auto-power spectra in the lateral mixing layers from the Renault Trafic at (2.0 m,1.0 m,0.5 m) (black line), (2.0 m,1.0 m,-0.5 m) (blue line). (*b*) Correlation (left scale, continuous line) and phase (right scale, dashed line) between the velocity signals at (2.0 m,1.0 m,0.5 m) and (2.0 m,1.0 m,-0.5 m).

IV. DISCUSSION

In order to reduce the drag of road vehicles through efficient design or control strategies, the mechanisms responsible for the low pressure on the base have to be clarified. The effects of the global mode structures and of the mixing layer characteristics are discussed respectively in Sections IV A and IV B.

A. Global modes

The presence of global modes in the wake is likely to impact the drag. In von-Kármán wakes past cylinders, most of the Reynolds stresses are related to the vortex shedding activity and the disturbance of the shear layer interaction is highly efficient to limit the global mode development and to reduce the drag[21]. Indeed, over such geometries, the mechanisms responsible for the closure of the recirculation region have a critical importance since the length of the mean bubble is directly linked to the base pressure[21,22]. In the experiments of Parezanović and Cadot[21] on the sensitivity analysis of the D-shape cylinder wake, the maximum of amplitude of the mode is located in the mixing layers before the end of the recirculation region for the undisturbed case whereas for optimal disturbed cases, this energy is then reported downstream the recirculation closure[23]. As a result, once efficiently disturbed, the mode seems less responsible for the closure of the recirculation which leads to an increased recirculation length and drag reduction.
The results presented in section III E highlight a coherent oscillations of the wake at least in the z direction over the Renault Trafic. The spectral analyzes show that the energy associated with this mode is small in comparison with the turbulent activity of the mixing layers, particularly upstream the end of the recirculation bubble. So, the contribution of these oscillating modes to the Reynolds stresses is limited and may not be sufficient to significantly affect the drag.

B. Mixing layer development

On the contrary, the mixing layer development certainly have a significant effect on the base pressure. Indeed, while it grows, the mixing layer incorporate fluid from the recirculation region; this leads to the curvature of the streamlines which is associated with low pressure in the wake, especially around the recirculating structures.
In the upper mixing layer, the low pressure is reported approximately at the middle of the recirculation in the x direction so it does not particularly affect the drag. For both vehicles, the lowest pressure on the base, *i.e.* the major contributors to the drag, are located in the lower part of the vehicle. In Section III D, it is shown that there is a huge difference between the upper and the lower mixing layers: the mixing layer from the roof presents the characteristics of the turbulent free shear flows and looses its structure at the end of the recirculation whereas the one out of the under-body has already lost the organization of a classical shear flow right downstream the separation. This absence of mixing layer organization from the under-body probably result from the fact that the flow in this region is highly three-dimensional and unsteady. For both mixing layers, the position of the low pressure in the wake seems to depend on the position where the shear flow looses its structure.
These results orient drag reduction strategies in two directions. First, a base pressure recovery should be observed once the bottom mixing layer restructured. Different means are possible such as reducing the ground clearance, limiting the under-body roughness or even getting a better evacuation of the air from the engine cooling. The second mean to reduce the base drag consists in controlling the mixing layer using active methods[24] or affecting the boundary layer before separation; the objective is to limit the growth rate $\mathrm{d}\delta_m/\mathrm{d}x$ at least close to the base. This would reduce the curvature of the streamlines and increase recirculation length leading to base pressure recovery.

V. CONCLUDING REMARKS

The flow around two different blunt vehicles is characterized at Reynolds number 10^7. First, the development of the boundary layer on the roof is depicted, it depends on the inclination of the roof that drives the pressure gradient along the vehicle. Then a massive recirculation responsible for a dominant part of the drag is reported on the base. The mean recirculating flow is highly dependent on the y direction, in particular the low pressure region is located close to the bottom part of the base whereas is has a reduced impact on the pressure on the top part. This may be explained by the differences between the upper and lower mixing layers: the upper one presents the characteristics of free shear flows in opposition to the mixing layer from the under-body. The spectral analyses also indicate the presence of a lateral oscillation of the wake but only past the Renault Trafic. However, this mode is not particularly energetic, its impact on the base pressure is certainly limited. This reduced global mode activity may be associated with the particularly high Reynolds numbers of the flow around such vehicles.
In a general prospect, these results may be used as a reference to orient the work on automotive drag reduction toward the control of the under-body flow in order to move the low pressure structure further downstream. A second control strategy could consist in reducing the growth rate of the mixing layer that should lead to base pressure

recovery and increased recirculation length.

Acknowledgments

The study has been performed by the CNRT R2A. This partnership between industrial and academical actors aims at providing comprehension and solutions to the aerodynamic and aeroacoustic issues of land vehicles.

[1] S. Ahmed, G. Ramm, G. Faitin, Some salient features of the time-averaged ground vehicle wake, Tech. rep., Society of Automotive Engineers, Inc., Warrendale, PA (1984).
[2] J. Beaudoin, O. Cadot, J. Aider, K. Gosse, P. Paranthoën, B. Hamelin, M. Tissier, D. Allano, I. Mutabazi, M. Gonzales, et al., Cavitation as a complementary tool for automotive aerodynamics, Experiments in fluids 37 (5) (2004) 763–768.
[3] W. Hucho, Aerodynamics of Road Vehicles, SAE, 1998.
[4] P. Gilliéron, A. Kourta, Aerodynamic drag reduction by vertical splitter plates, Experiments in fluids 48 (1) (2010) 1–16.
[5] J. Beaudoin, J. Aider, Drag and lift reduction of a 3D bluff body using flaps, Experiments in Fluids 44 (4) (2008) 491–501.
[6] G. Fourrié, L. Keirsbulck, L. Labraga, P. Gilliéron, Bluff-body drag reduction using a deflector, Experiments in Fluids 50 (2) (2011) 385–395.
[7] G. Pujals, S. Depardon, C. Cossu, Drag reduction of a 3d bluff body using coherent streamwise streaks, Experiments in fluids 49 (5) (2010) 1085–1094.
[8] C. Bruneau, E. Creuse, D. Depeyras, P. Gillieron, Active procedures to control the flow past the ahmed body with a 25° rear window, International Journal of Aerodynamics 1 (3) (2011) 299–317.
[9] B. Khalighi, S. Zhang, C. Koromilas, S. Balkanyi, L. Bernal, G. Iaccarino, P. Moin, Experimental and computational study of unsteady wake flow behind a bluff body with a drag reduction device, SAE paper.
[10] R. Littlewood, M. Passmore, The Optimization of Roof Trailing Edge Geometry of a Simple Square-Back., SAE paper.
[11] C. Bruneau, E. Creusé, D. Depeyras, P. Gilliéron, I. Mortazavi, Coupling active and passive techniques to control the flow past the square back ahmed body, Computers & Fluids 39 (10) (2010) 1875–1892.
[12] E. Duell, A. George, Experimental study of a ground vehicle body unsteady near wake, SAE transactions 108 (6; PART 1) (1999) 1589–1602.
[13] I. Bayraktar, D. Landman, O. Baysal, Experimental and computational investigation of ahmed body for ground vehicle aerodynamics.
[14] P. Waudby-Smith, T. Bender, R. Vigneron, The gie s2a full-scale aero-acoustic wind tunnel, SAE transactions 113 (6) (2004) 449–461.
[15] N. J. Lawson, K. P. Garry, N. Faucompret, An investigation of the flow characteristics in the bootdeck region of a scale model notchback saloon vehicle, Proceedings of the institution of mechanical engineers PART D-journal of automobile engineering 221 (D6) (2007) 739–754.
[16] M. Grandemange, V. Parezanović, M. Gohlke, O. Cadot, On experimental sensitivity analysis of the turbulent wake from an axisymmetric blunt trailing edge, Physics of fluids 24 (2012) 035106.
[17] F. Champagne, Y. Pao, I. Wygnanski, On the two-dimensional mixing region, Journal of Fluid Mechanics 74 (02) (1976) 209–250.
[18] P. Dimotakis, Turbulent free shear layer mixing and combustion, High Speed Flight Propulsion Systems (1991) 265–340.
[19] S. Pope, Turbulent flows, Cambridge Univ Pr, 2000.
[20] A. Hussain, K. Zaman, An experimental study of organized motions in the turbulent plane mixing layer, Journal of Fluid Mechanics 159 (1) (1985) 85–104.
[21] V. Parezanović, O. Cadot, Experimental sensitivity analysis of the global properties of a 2D turbulent wake, Journal of Fluid Mechanics 693 (2012) 115–149.
[22] A. Roshko, Perspectives on bluff body aerodynamics, Journal of Wind Engineering and Industrial Aerodynamics 49 (1-3) (1993) 79–100.
[23] O. Cadot, B. Thiria, J. F. Beaudoin, Passive drag control of a turbulent wake by local disturbances, Vol. 14 of IUTAM Bookseries, 2009, pp. 529–537, iUTAM Symposium on Unsteady Separated Flows and their Control, Corfu, GREECE, JUN 18-22, 2007.
[24] D. Greenblatt, I. Wygnanski, The control of flow separation by periodic excitation, Progress in Aerospace Sciences 36 (7) (2000) 487–545.